

Journal of the Geological Society

The tectonic setting and earthquake ground hazards of the 1993 Pyrgos earthquake, Peloponnese, Greece

I. KOUKOUVELAS, A. MPRESIAKAS, E. SOKOS and T. DOUTSOS

Journal of the Geological Society 1996; v. 153; p. 39-49
doi:10.1144/gsjgs.153.1.0039

Email alerting service

[click here](#) to receive free email alerts when new articles cite this article

Permission request

[click here](#) to seek permission to re-use all or part of this article

Subscribe

[click here](#) to subscribe to Journal of the Geological Society or the Lyell Collection

Notes

Downloaded by

University of Patras/Library and Information Center on 27 June 2008

The tectonic setting and earthquake ground hazards of the 1993 Pyrgos earthquake, Peloponnese, Greece

I. KOUKOUVELAS, A. MPRESIAKAS, E. SOKOS & T. DOUTSOS
Department of Geology, University of Patras, Patras, 26110 Greece

Abstract: The Pyrgos earthquake in western Greece (26 March 1993) ($M_L = 5.2$) was caused by oblique-normal slip on a north-dipping and WNW-trending fault, and produced significant damage in the town of Pyrgos. Several lines of evidence from the epicentral area suggest that faults within two active grabens in the Pyrgos basin, the Grape and Alfios grabens, were reactivated during this earthquake and subsequent aftershocks. Evaluation of morphotectonic data, the fault slip-rate between 0.05 and 0.35 mm a⁻¹ and seismic activity associated with the 1993 earthquake, suggest that the Alfios graben is the most active structure in the basin. This graben, which is 25 km long and crosses the Pyrgos basin, is segmented along its strike by transfer zones. Analysis of the seismic activity in this graben shows that transfer zones are the focus for the concentration of seismic activity and thus the concept of transfer zones is important for understanding the Pyrgos earthquake.

The 1993 earthquake caused landslides at 47 locations and liquefaction phenomena at 7 localities within an area of 145 km². The lower threshold level to induce landslides was $M_L = 4.0$ and to induce liquefaction was 5.0. The majority of landslides occurred along fault scarps and either caused the slope to retreat and/or acted to protect the slope gradient.

Keywords: Greece, normal faults, segmentation, earthquakes, graben.

On 26 March 1993, a moderate magnitude earthquake occurred in the vicinity of Pyrgos town, western Greece (Figs 1 & 2). This earthquake, here called the 'Pyrgos earthquake', had a local magnitude $M_L = 5.2$ with a hypocentre at a depth of 10 km, and caused landslides within an elliptical area 145 km², which occupies the central part of the Pyrgos basin (Figs 1a and 2a).

Local magnitude (M_L) quantifies the earthquake size measured by analysis of recorded seismic wave amplitude: obtaining the maximum seismic wave amplitude, measuring the distance from the earthquake source and comparing the earthquake to a reference earthquake (Richter 1935). Magnitude is the logarithm to base 10 of maximum wave amplitude.

The Pyrgos basin lies along the western shore of the Peloponnese and contains a post-upper Miocene sedimentary sequence (Fig. 2b), which unconformably overlies a west-verging stack of flat-lying nappes (Hageman 1976; Jacobshagen 1986).

The study area is situated 55 km east of the northwesternmost end of the Hellenic subduction zone (Fig. 1a, b), where orthogonal convergence between the African and the European plate is occurring (McKenzie 1972; Mercier *et al.* 1972; Doutsos *et al.* 1987; Underhill 1989; Jackson 1994). The geometry of the subducting plate is gently sloping under the Peloponnese and steepens abruptly under the Corinthos area (Papazachos & Comninakis 1971; Leydecker *et al.* 1978; Hatzfeld *et al.* 1990) (Fig. 1d). Two subduction-related seismotectonic regimes can be recognized: (1) a trenchward compressional regime incorporating the Ionian islands and (2) an extensional back-arc regime including central mainland Greece, the Aegean islands and the Peloponnese. Extension within the back-arc area is accommodated mainly by WNW-trending seismogenic

normal faults, typically from 10 to 15 km in length (Roberts & Jackson 1991). Slip rates along these faults reach up to 1.5 mm a⁻¹ (Doutsos & Piper 1990; Doutsos & Poulimenos 1992; Roberts *et al.* 1993) resulting in a total rate of extension, in central Greece, between 40–60 mm a⁻¹ (McKenzie 1978; Le Pichon & Angelier 1979; Jackson & McKenzie 1988; Ambraseys & Jackson 1990).

Historical records and instrumental seismicity attest to the frequent occurrence of destructive earthquakes along the northern and the southern margins of the Peloponnese (Papazachos & Papazachou 1989; Ambraseys & Jackson 1990) (Fig. 1c). The study area itself is notable for its historical paucity of large ($M_L > 6.0$) surface-faulting earthquakes (Ambraseys & Jackson 1990). The typical magnitude of the onshore seismicity in the Peloponnese is $M_L \approx 5.2$, with a maximum magnitude of 5.9 in the Megalopolis 1965 earthquake (Ambraseys & Jackson 1990). Figure 1c shows the distribution of earthquakes in the Peloponnese that occurred during the period 1911–1979 (after Papazachos & Comninakis 1982). Directly comparable geographical distributions of small magnitude earthquake epicenters are also reported by Leydecker *et al.* (1978) and Hatzfeld *et al.* (1989) (Fig. 1c) recorded by portable networks.

In this paper, we present an interpretation of threshold intensities needed to induce ground hazards in the Pyrgos area of western Greece, a seismotectonic interpretation of this area, and a description of denudation processes produced by earthquake triggered landslides on fault scarps. Furthermore, by integrating regional tectonic data, detailed structural data and earthquake information, we reconstruct the geometry of the deformation along the western part of Peloponnese. In order to understand the relationship between displacement on faults and seismicity in a

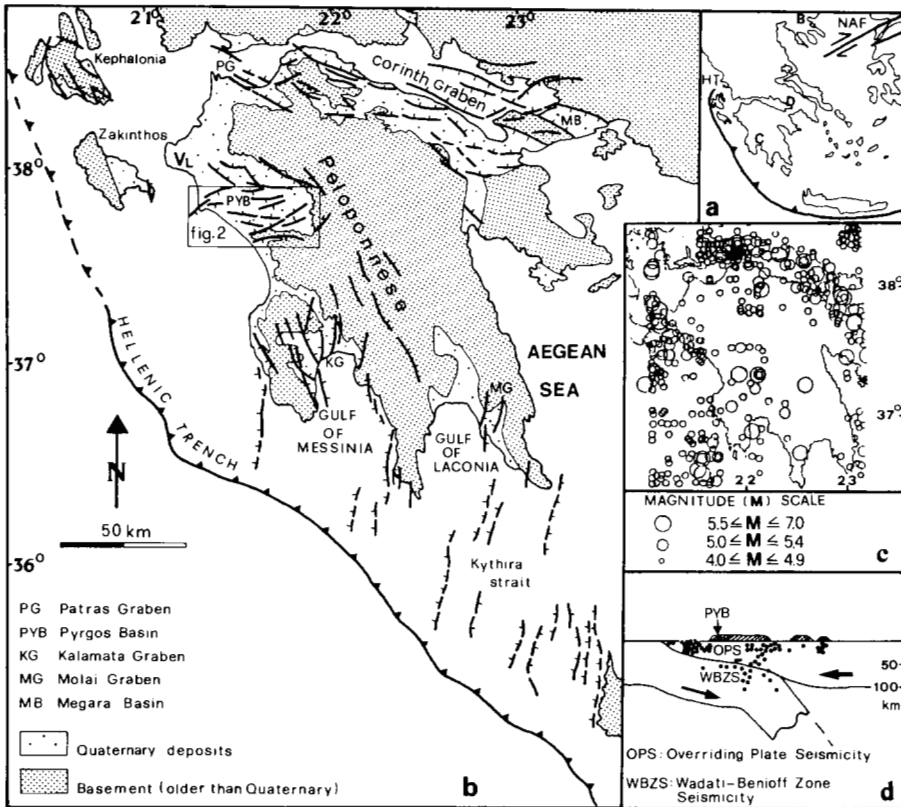


Fig. 1. (a) Map showing the position of the study area in relation to the Aegean province. (NAF) North Anatolian Fault, (HT) Hellenic Trench, (B) Thessaloniki earthquake, (C) Kalamata earthquake and, (D) Corinthian earthquakes (see Fig. 9). (b) General tectonic setting of Peloponnese with outline of Quaternary tectonics. Pyrgos Basin in rectangle. (data for Corinthian graben: Jackson *et al.* 1982, Zeligidis *et al.* 1989, Doutsos & Poulimenos 1992 and Papatheodorou & Ferentinis 1993; data for Kalamata graben and Kythira strait: Lyon-Caen *et al.* 1988, Zeligidis & Doutsos 1992, Armijo *et al.* 1992; data for Zakynthos and Kephallonia: Underhill 1989; data for Pyrgos basin: A. M. unpublished mapping). (c) Seismicity map of Peloponnese (after Papazachos & Comninakis 1982). (d) Cross-section defining terminology for earthquake classification (modified after Hatzfeld 1994), (PYB) Pyrgos Basin.

structurally complex basin like the Pyrgos basin, we compare this area with other seismotectonic areas of Greece.

Stratigraphy of the Pyrgos Basin

The Pyrgos basin fill comprises two sedimentary systems. The *lower sedimentary system* consists of the marine-lacustrine Platana and Vounargos formations (Hageman 1976; Fig. 2b). An overall coarsening-up trend characterizes both formations. The 150 m thick Platana Fm was deposited during the Late Miocene (Fig. 2b). Higher up, the lacustrine and marine sediments of the Platana Fm are interdigitated basinwards with the overlying Vounargos Fm. Plant fossils in the Platana Fm suggest an axial entrance of the sea parallel to the Lapithas mountain during the Late Miocene (Kleinholter 1994). Small-scale fan deposits across the Lapithas high and an axial influx of fluvial sediments are observed in the upper part of the Platana Fm, indicating the onset of the Vounargos deposition and the rapid uplift of the basin. The overlying Vounargos Fm, up to 1000 m thick, is the main lithological unit in the basin (Hageman 1976; Kamberis 1987). It is of Piacentian age (Frydas 1987). Sedimentological data on the Vounargos Fm (Hageman 1976, and this study) suggest that the boundary between marine-lagoonal environments is defined by asymmetrical fault-bounded sand lenses. Several influx points are identified where sediments derived from limestone on the eastern margin were discharged into the basin (Fig. 2a). The Pliocene Vounargos depocentre extends in an east-west direction. This transition from lagoonal to shallow marine deposits is considered analogous to the features observed in the shoreward lagoons and adjacent, shallow marine areas of

the modern gulf (Kyparissiakos Gulf) which are separated by elongate sand bodies in the form of NW-trending beaches and sand dunes (Fig. 2).

The *upper sedimentary system* consists of three formations. At the bottom, the 200 m thick Pliocene Olympia Fm is a coarsening-up fluvio-lacustrine succession overlain by the 400 m thick Erymanthos conglomerates (Hageman 1976), with sediment supply for both formations being from the north (Fig. 2). On the top of this system the 80 m thick Middle Pleistocene-Holocene Alfios Fm is exposed in the low-land area of the Pyrgos basin (Fig. 3).

Tectonic aspects

Stress field

The Pyrgos basin developed as a complex basin affected by Pliocene syndimentary faults, trending both parallel (NW) and perpendicular (NE) to the isopic zones of the Hellenides. Faults of Pliocene age are recognized as highly eroded fault scarps or as buried faults controlling Vounargos and Platana Formation facies changes. Slickenside lineations on the fault planes (Fig. 4 net A) indicate that the direction of the least compression, σ_3 , is NW-SE. In order to determine the stress tensor responsible for the kinematics of this fault population we carried out computer calculations using a computer program (for numerical palaeostress reconstructions methods see Carey & Brunier 1974; Etchecopar *et al.* 1981 and Oncken 1988).

A later fault system, formed at the beginning of the Quaternary period, produces WNW-trending asymmetrical graben. Fault plane and slickenside lineation data for these faults indicates that the direction of least compression, σ_3 , is

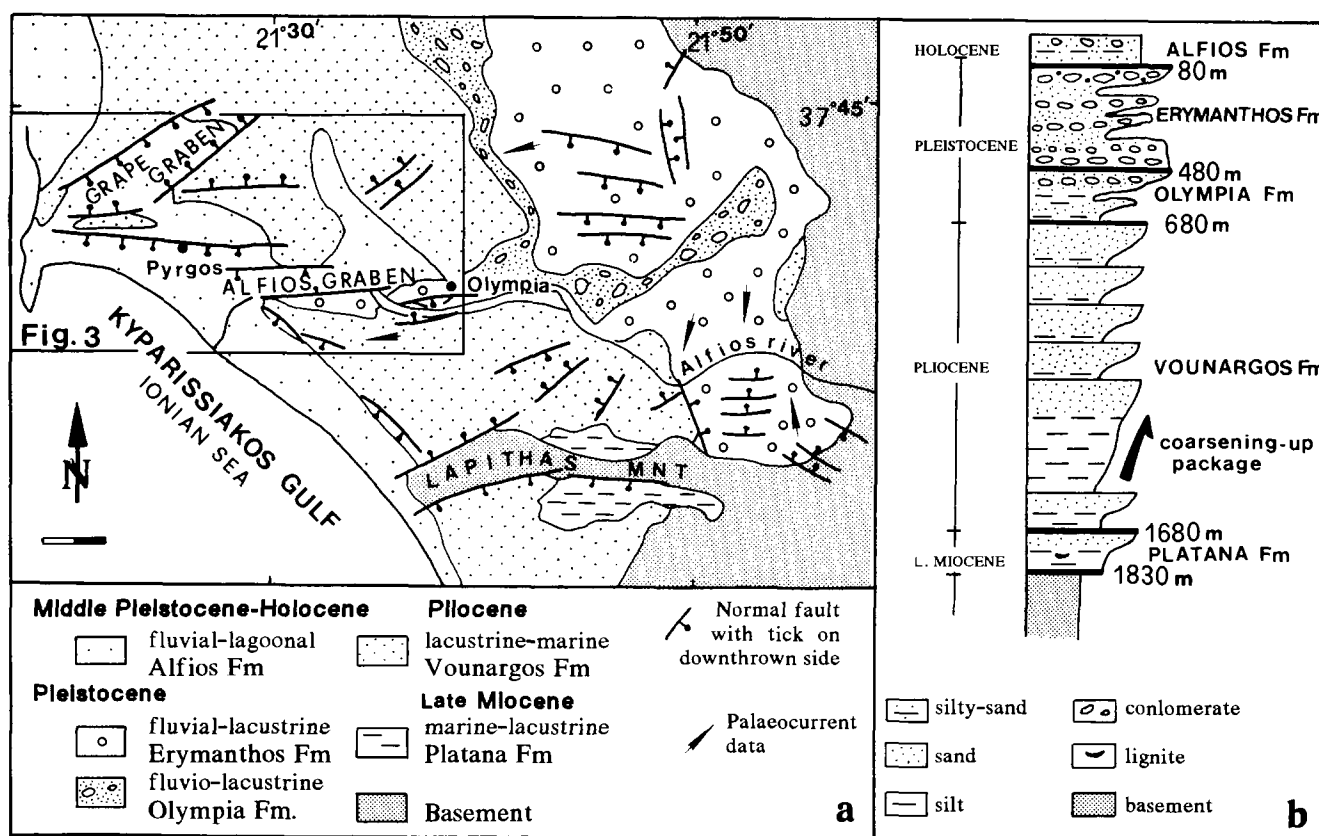


Fig. 2. (a) Simplified geological map of the Pyrgos Basin, including major faults and structures. (b) Synoptic stratigraphic column in the Pyrgos Basin. The Platana Fm and the upper part of the Vounargos Fm and Olympia Fm are defined following Hageman (1976). The lower part of the Vounargos Fm is defined following Kamberis (1987). Age definitions are after Hageman (1976).

NNE-SSW (Fig. 4 net AG) comparable to that reported for the USGS focal plane solution for the 1993 Pyrgos earthquake (Fig. 3).

Pliocene faults and newly formed faults in the area of the Grape graben have been active during NNE-SSW extension, resulting in complicated reactivations (Fig. 4 net GG). Fault plane and slickenside lineation data for faults in this area indicate that the older NW- and NE-trending faults underwent oblique, left-lateral and normal reactivation, and newly formed dip-slip normal faults were developed in this area during the Quaternary period (Fig. 4 net GG).

Normal faulting, slip rates and correlation with topography

Deformation of the study area has involved newly-formed structures, e.g. the Alfios graben and the Lanthi fault, of Quaternary age, and older reactivated structures, e.g. the Grape graben and the Pyrgos fault, of Pliocene age. A 40 km long extensional structure consisting of the Alfios graben and the Pyrgos fault delimits the southern part of the Pyrgos basin (Fig. 2a).

The WNW-trending Alfios graben, of dimensions 3 km by 25 km (Fig. 2a), is characterized by recent sedimentation in the area along the Alfios river. This study examines the western part of the Alfios graben; (Fig. 3, cross section AB) an area reactivated by ruptures at depth during the Pyrgos earthquake. The south-facing Varvasaina fault has a slip rate

0.14 mm a^{-1} (Table 1). The north-facing Alfiooussa fault has a throw of 220 m, between erosion surface (120 m high) in the footwall to the south, and the base of the Alfios graben (100 m below sea level, borehole data). The age of initiation of displacement on the Alfiooussa fault is estimated to be as young as the deposition of Alfios Fm (700 ka). This age is based on the assumption that similar sediments at the north Peloponnese (Doutsos *et al.* 1987; Zelilidis *et al.* 1988) are biostratigraphically dated as Middle Pleistocene (Symeonidis *et al.* 1987; Moutzos 1990). Based on these data a slip rate of 0.31 mm a^{-1} is suggested for the Alfiooussa fault (Table 1).

Time-averaged slip rates for vertical movement have been calculated for datable faults. Slip rates have been determined from total geological offset (defined by sediment thickness, height of fault scarp, and erosion) divided by the age of the fault (biostratigraphical ages). For a more complete discussion of the method see Doutsos & Piper (1990). Biostratigraphical data for the base of Vounargos, Piacentian, are from Tsaila-Monopolis *et al.* (1993), and data for Holocene sediments from Symeonidis *et al.* (1987), Moutzos (1990). Quoted uncertainties reflect ambiguities of displacement measurements caused by the accuracy of topographic maps, accuracy of geophysical methods and errors of drilling depth. Additional uncertainties are caused by biostratigraphical ages. Based on these parameters, data, uncertainties and errors in slip-rate ratios for datable faults are tabulated (Table 1).

The overall topography of the Alfiooussa fault footwall area is dominated by steep north facing scarps extending for

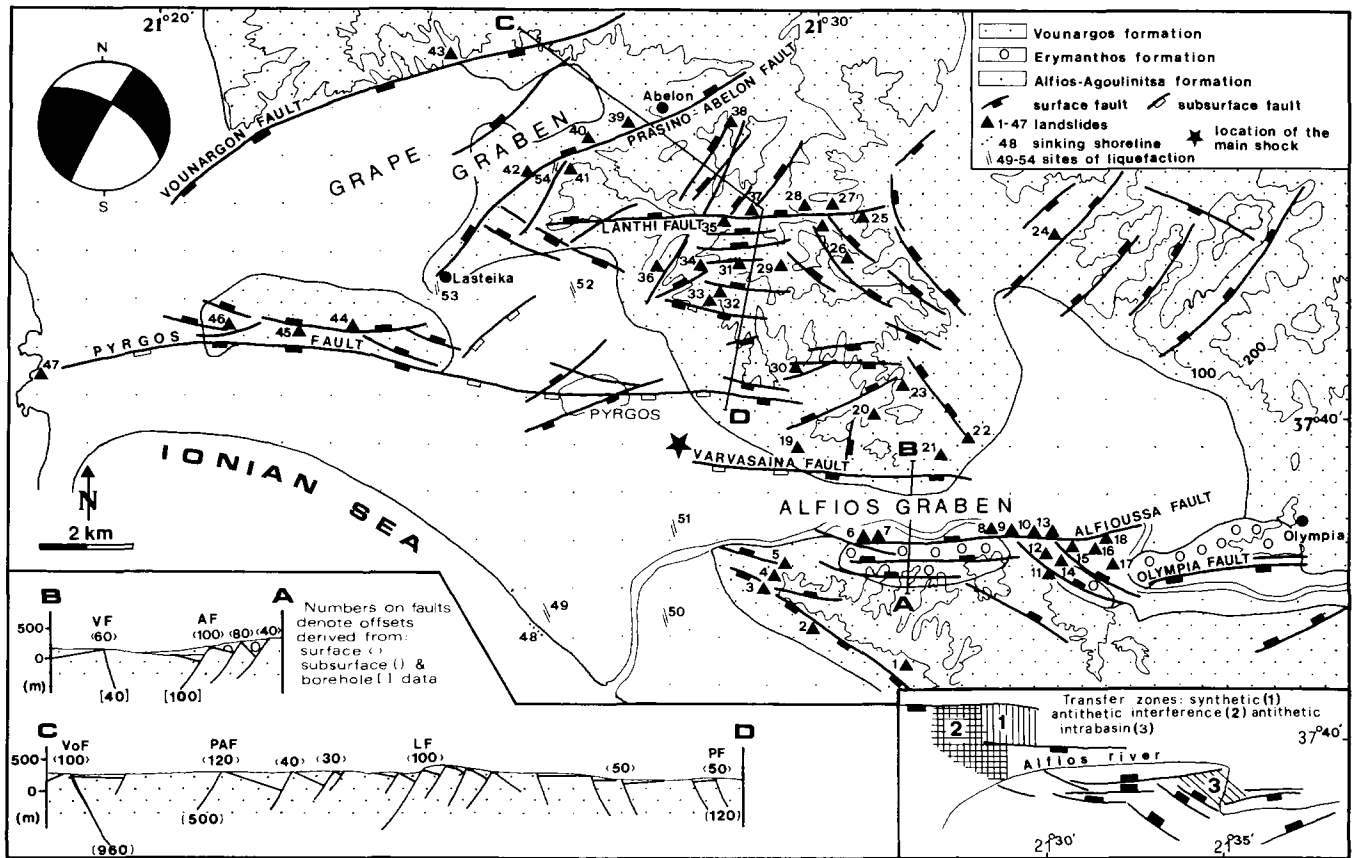


Fig. 3. Tectonic and ground hazard map of the area affected by the Pyrgos earthquake. Inset shows the classification of transfer zones (*sensu* Gawthorpe & Hurst 1993) between the Pyrgos, Varvasaina, Alfiooussa and Olympia faults. Focal mechanism is shown as lower-hemisphere equal-area projection (data after USGS).

1.5 to 6.5 km in length with 10–70 m high escarpments. We interpret this steepness as evidence of recent activation of the faults. The overlapping east termination of the Alfiooussa fault with the Olympia fault forms an intrabasin ridge (*sensu* Gawthorpe & Hurst 1993) (inset of Fig. 3, 3). An

underlapping interference zone (*sensu* Gawthorpe & Hurst 1993) defines the west termination of the Alfiooussa and Pyrgos faults (inset of Fig. 3, 2). This zone discharges sediments onto the Alfios delta plain from a point source.

The 18.1 km long south-facing Pyrgos fault, segmented

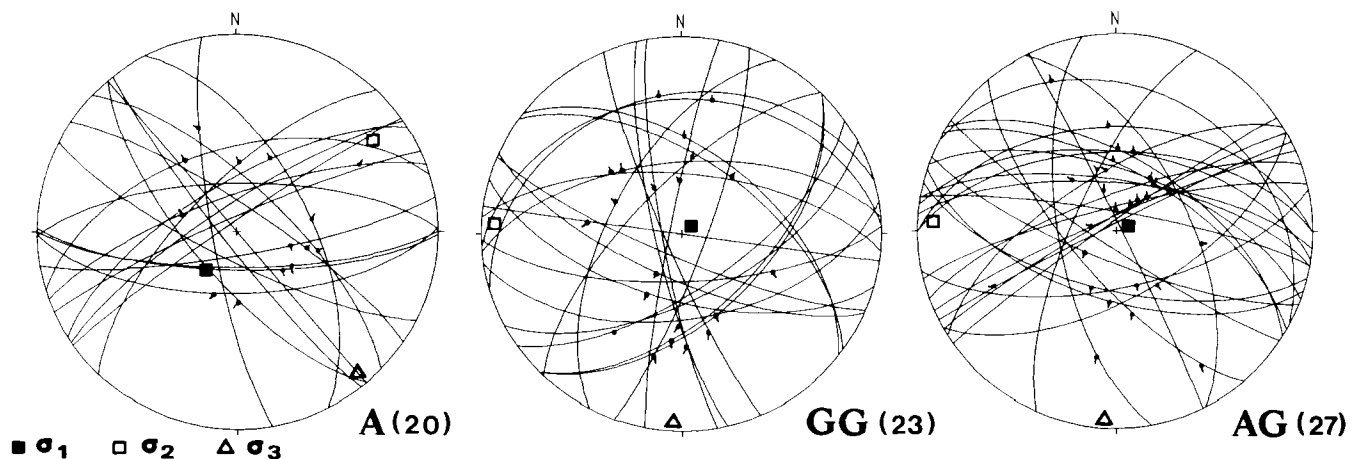


Fig. 4. Lower-hemisphere equal-area projections of slip plane (cyclographic traces) and associated striations (dots with ticks) for (A) Vounargos and Platana Formations (number of faults is 20), (GG) Grape graben (number of faults is 23), (AG) Alfios graben (number of faults is 27). Principal stresses σ_1 , σ_2 , σ_3 are shown as solid square, open square, and open triangle respectively. All faults have a normal slip component.

Table 1. Estimates of displacement and slip-rate for selected faults in the Pyrgos basin

Faults	Stratigraphy	Displacements* (m)	Displacement errors (m)	Assumed age (Ma)†	Age errors (Ma)	Slip rate ratios (mm a ⁻¹)	Errors (mm a ⁻¹)
Vounargon	Base of Vounargos Fm	(960)	(15)	3.4	±0.2	0.35	+0.04/-0.03
	Base of Alfios Fm	<100>	<20>	0.7	±0.2	0.14	+0.1/-0.06
Prasino-Abelon	Base of Vounargos Fm	(120) (500)	<20> (15)	3.4	±0.2	0.18	±0.02
Pyrgos	Base of Vounargos Fm	<50> (120)	<20> (15)	3.4	±0.2	0.05	+0.01/-0.02
Varvasaina	Younger than the deposition of Alfios Fm	<60> [40]	<20> [5]	0.7	±0.2	0.14	+0.11/-0.06
Alfioussa	Younger than the deposition of Alfios Fm	<120> [100]	<20> [5]	0.7	±0.2	0.31	+0.18/-0.1

* The measured vertical displacements are derived from < > surface, () subsurface and [] borehole data.

† Rates are estimated by assumed biostratigraphic chronology.

along its strike at the surface (Fig. 3), passes through the town of Pyrgos and has a maximum displacement of 170 m. Piacentian to recent deposition of sediments adjacent to the Pyrgos fault shows that this fault has been active from Piacentian time (offsetting the Piacentian basal Vounargos Fm and forming fresh scarps), and its slip rate is calculated at 0.05 mm a⁻¹. A synthetic transfer zone (*sensu* Morley *et al.* 1990) defines the termination of Pyrgos and Varvasaina faults that tilted the intervening basin floor to the west (in Fig. 3, 1).

The 8 km long Lanthi fault, which is of the step-type and faces north, forms relief 10 m to 70 m high with steep fault scarps. As the Lanthi fault truncates all the NE- and NW-trending faults and drops the erosion surface to the north by 100 m, it is the most recently active fault in the hilly countryside (Fig. 3, cross section CD).

The ENE-trending Grape graben (Fig. 3), of dimensions 3 km by 10 km, was reactivated by ruptures at depth during the last earthquake sequence. This graben is defined to the north by the Vounargon fault, which has a total maximum throw of ≤1060 m, and to the south by the Prasino-Abelon fault which has a total maximum throw of 620 m and a slip rate of 0.18 mm a⁻¹. A continuous temporal decrease of the slip rate from 0.35 mm a⁻¹ during the Pliocene (960 m throw during the time interval from 3.4 Ma to 0.7 Ma) to 0.14 mm a⁻¹ during the Quaternary is calculated on the Vounargon fault. The total throw of the Vounargon fault is calculated as the thickness of Vounargos Fm plus the height of fault scarp, with data showing the subsurface configuration of the base of Vounargos Fm from Kamberis (1987). The 8.5 km long north facing Prasino-Abelon fault is here interpreted as a master step-type fault with three high-angle faults parallel to the Prasino-Abelon fault which have uplifted their footwalls by as much as 50 m, forming low scarps.

The above mentioned data suggest that throughout the study area the north-facing scarps are associated with larger displacements than south-facing scarps, resulting in a net lowering of the northern block, with the Vounargon fault ultimately terminating this tectonic framework to the north.

Seismic activity

The local magnitude $M_L = 5.2$ Pyrgos earthquake was accompanied by spatially scattered foreshock and aftershock activity. In this section, the spatial distribution of the

aftershock activity is described in detail, with particular attention paid to the temporal distribution.

In Fig. 5 we show, for the Pyrgos earthquake, the main shock epicentre, and the epicentres of all associated seismic activity ($M_L > 2.5$) possessing high quality epicentral locations. Earthquake hypocentres were determined using the routine HYPO 71 of Lee & Lahr (1972). We also used the horizontally-layered velocity model suggested for Western Greece by Hatzfeld *et al.* (1990). All events in Fig. 5 have precision errors as follows: root square traveltimes residual (rms) < 0.28 s, horizontal errors (ERH) < 3.0 km and vertical errors (ERZ) < 3.6 km.

The earthquake activity in the area of Pyrgos started with a foreshock ten minutes before the main event ($M_L = 4.8$, Fig. 5 event 1), while the main shock was recorded as the last member of a three-event swarm. The first ($M_L = 2.8$) and the second ($M_L = 4.0$) events of the swarm were three and two minutes ahead of the main event respectively (Fig. 5 events 2,3). The epicentral positioning of

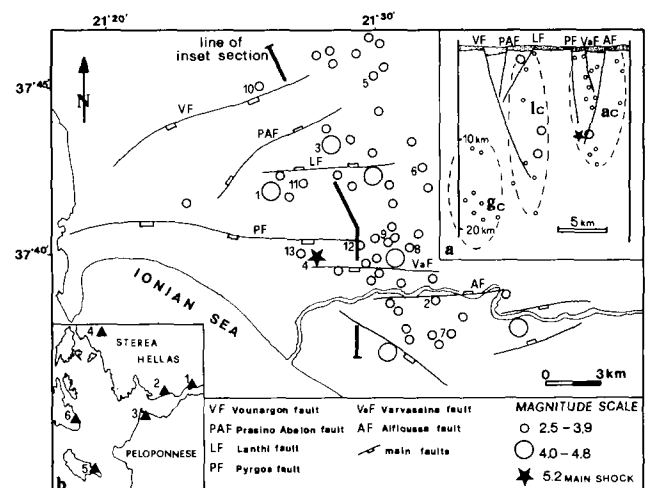


Fig. 5. Map showing main shock and aftershocks (54 events) located in the area affected by the Pyrgos earthquake. Numbering from 1–13 indicates the temporal sequence in a time span of 2 hours. (a) Cross-section showing the association of swarm seismicity with the tectonic structure, which consists of normal faults. (b) Map showing the six stations of the Patras network (station 1 Nafpaktos, 2 Varasova, 3 Papas, 4 Akarnanika, 5 Zakynthos, 6 Kefalonia).

these events, taking part on different rupture surfaces close together in time (*sensu* Scholz 1990), means that the Pyrgos earthquake can be classified as a compound earthquake. Two hours after the main event (Fig. 5, sequential numbering) the aftershocks were scattered over a wide area. The depth distribution of upper-crustal earthquakes was apparently controlled by Pliocene and Quaternary normal faults (Fig. 5 inset A). Later aftershocks defined three clusters with intense seismicity.

The three clusters are located in the Alfios and Grape grabens and in the area around the Lanthi fault. In the *Alfios cluster*, hypocentres are located at depths ranging from 1 to 8 km (ac in Fig. 5). This cluster is also characterized by a shifting of the hypocenters towards ancient Olympia, as delineated by the $M_L = 4.2$ event two weeks later after the main event. In the *Lanthi cluster*, hypocentres are located at depths ranging from 1 to 18 km (lc in Fig. 5), and the seismicity is scattered in map view, expressing the structural complexity of this area. Since the Lanthi fault is the most active fault in this area, most of the shallow shocks may be related to this fault. The Grape graben is a structurally simple area and there is a tendency for events to cluster at the northeast end of the Prasino-Abelon fault. Most focal depths from the *Grape cluster* occurred in the depth range 15 to 20 km (gc in Fig. 5).

Hazards analysis

Earthquake triggered landslides

Earthquakes can affect epicentral areas in terms of landsliding and/or soil lateral spreading (Keefer 1984). However, as down-slope movements are triggered by variable factors, i.e. climate, slope shape, vegetation etc. (see Terzaghi 1950), our goals were to analyse landslides exclusively triggered by the earthquake activity. In order to clarify the relationship between landslides and earthquake activity, we analyzed the geomorphology and the climatological data, and compared old landslides to earthquake-triggered landslides.

A series of 47 earthquake-triggered landslides and seven sites of soil lateral spreading were mapped after the Pyrgos

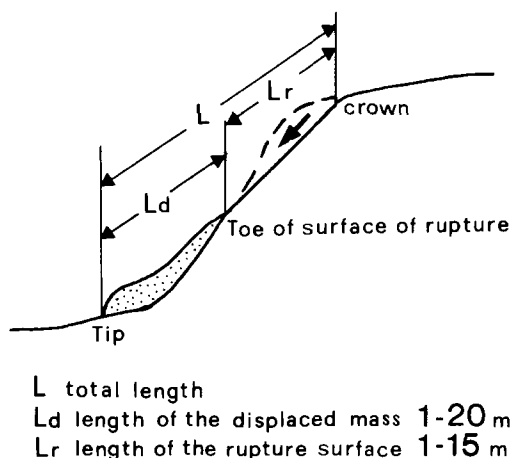


Fig. 6. Geometrical characteristics of the earthquake triggered landslides during the Pyrgos earthquake. (Modified after the IAEG 1990).

earthquake (Fig. 3). These landslides are recognized as small-scale mass movements (Fig. 6), belonging to three families: soil falls (23 sites), soil block slides (18 sites) and soil slides (6 sites) (classification *sensu* Keefer 1984). Earthquake-triggered landslides and soil lateral spreading are observed within an onshore elliptical area of 145 km² with its long axis in a WNW-direction (Fig. 7a). This area is separated into two, differentiated by the presence of liquefaction sites (inner) and of sliding sites (outer) (Fig. 7a). Thus the area affected by landslides versus the earthquake magnitude (Fig. 7b, point P) and the maximum distance of liquefaction versus earthquake magnitude (Fig. 7c, point P) on Keefer's (1984) plots can be used for labelling the two contours in Fig. 7a. These plots shows that the outer limit corresponds to the threshold for earthquake-triggered landslides is $M_L = 4.0$ and the inner limit corresponds threshold for liquefaction sites is $M_L = 5.0$ (Fig. 7a).

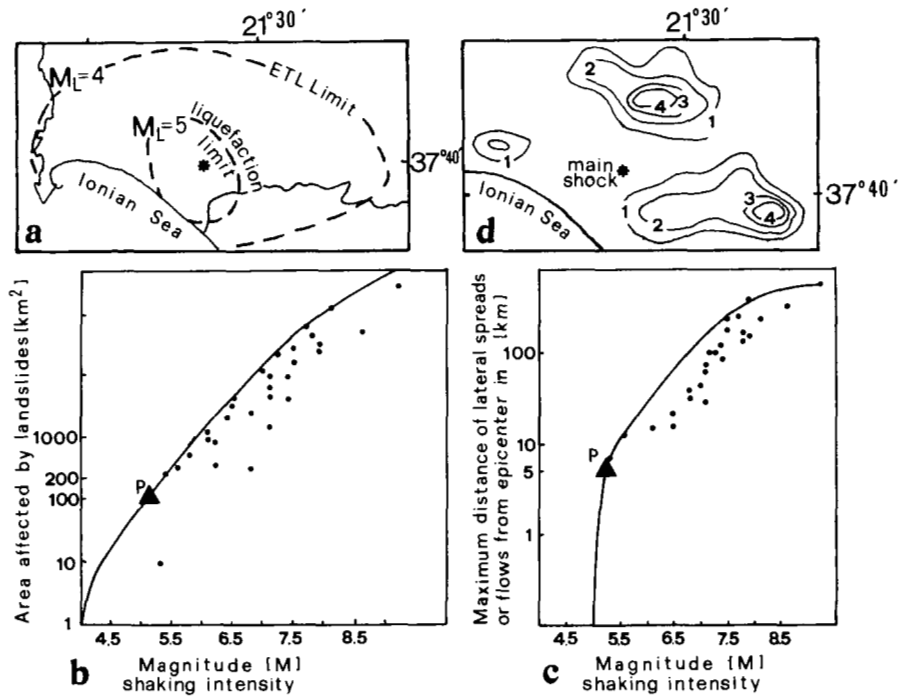
Earthquake-triggered landslides are observed in the hilly countryside east of Pyrgos town, which shows the typical characteristics of badlands slopes. This geomorphic form of the study area is controlled by a drainage system that is downcutting highly erodible materials (i.e. Vounargos sands) and produces deep valleys which have then widened by lateral erosion. The drainage system of Pyrgos hilly countryside has been analyzed using the method of Strahler (1975), in which the channel network is divided into segments and assigned a channel order. The ratio between the number of segments of any given order to the number of segments of the next higher order is the Bifurcation ratio (Strahler 1975). The average bifurcation ratio for the Pyrgos hilly countryside is 3.47, with individual basins ranging from 2.57 to 4.37; the latter value being interpreted as indicating a mature drainage network.

Landslide occurrence in the epicentral area shows strong relationships with north- to northeast-facing slopes. The slope aspect, the direction in which slopes face, dictates chute-facing direction subparallel to active faults (Figs 3 & 4). Thus the strong aspect control results from structural rather than climatic factors. Earthquake triggered landslides in the Pyrgos earthquake epicentral area occurred preferentially on fault scarps (85%) (Figs 7d and 8 types A,B,C) or in gullies (15%) (Fig. 8 type D), with a safety factor $F_s = 0.9$, which indicates retreating fault scarps. The safety factor is the ratio between force that indicates resistance of the rock to slide, to the force that triggers sliding (definition after Hoek & Bray 1977). A factor $F_s = 1$ represents the point of failure, while values greater than unity characterize stable slopes. The safety factor number is calculated by using the formula of Skempton & DeLory (1957), the data for effective stress value (c) and the angle of internal friction (ϕ) from Andronopoulos & Koukis (1977).

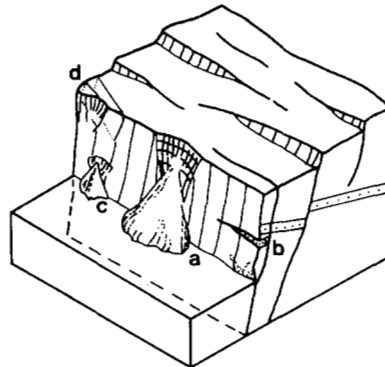
Climatological data for the ten-year period prior to the earthquake can be summarized as follows: average spring temperature approximately 6 to 16°C, annual average precipitation as much as 950 mm, and average March precipitation 86 mm. Heavy rainfall took place on 27 March 1993, one day after the main shock, followed by showers, with winds blowing from the southwest. Thus the landslides occurred in dry rocks.

The area affected by earthquake-triggered landslides were mapped three times during the one month period after the main event, in order to describe any possible evolution of all sliding sites with the evolution of the seismic activity.

Fig. 7. (a) Threshold levels of shaking intensities (M_L) based on the distribution of ground hazards. (b) Plot indicating the area affected by landslides versus magnitude of surface shaking; solid triangle, labeled as (P), corresponds to Pyrgos earthquake, solid dots after Keefer (1984). (c) Plot indicating maximum distance of liquefaction sites versus magnitude of surface shaking; solid triangle, labelled as (P), corresponds to Pyrgos earthquake, solid dots after Keefer (1984). (d) Map constructed from geographical distribution of earthquake triggered landslides that occur over epicentral area. The contouring is showing population density of landslide deposits. The isopleth map of landslides is based on 2.5×2.5 km data grid.



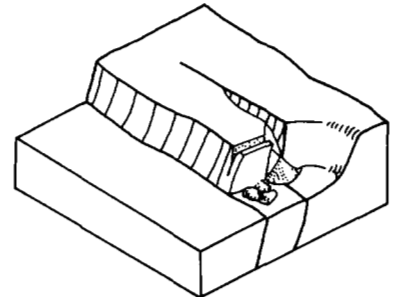
Type A Slides along step type fault



a: spalling-off masses, b: peeling-off sheets
c: wedge-shaped slides, d: tension cracks

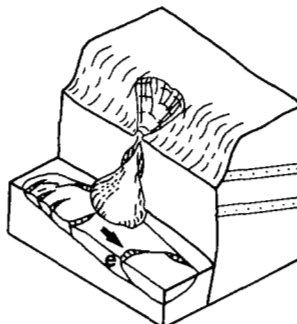
Sites: 1,2,3,4,5,6,7,8,9,10,11,12,13,14,15,
18,20,21,27,41,42.

Type B Toppling and wedging on a fault



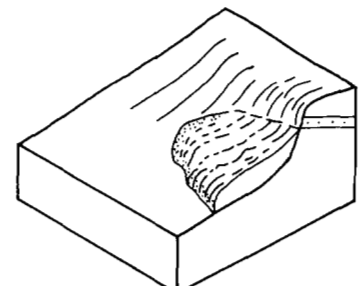
Sites : 16,17,22,23,26,28,29,33,34,35,
36,37,44,45,46,47.

Type C Wedge failure forming tear drop talus



e: old landslide along the strike of the fault scarp
Sites : 24,25,30,38,39,43.

Type D: Coherent rotational slump



Sites: 19,31,32,40.

Fig. 8. Block diagrams indicating the prominent mechanism of retreating and/or protecting processes on each fault type during the Pyrgos earthquake (see text for explanation). The numbers in each block diagram refer to sites located in Fig. 3. Arrow in block diagram of Type C showing the sense of movement of the old landslide.

Repeated field mapping has shown that all earthquake-triggered landslides are new and that they took place in materials not previously involved in landslides. Remapping all earthquake-triggered landslides nine months after the main event showed that all earthquake-triggered landslides are stable. In one particular case where an earthquake-triggered landslide had developed over an old landslide, the two slides show different mechanisms of formation, sense of movement and geometry (Fig. 8 type C). In this example, the old landslide moved seasonally along the strike of the fault scarp over a subhorizontal shallowly-dipping detachment plane. The earthquake triggered landslide, once originated, denuded the near-top of the fault scarp, moving quickly downwards and outwards.

As the aftershock activity was expressed by events close to $M_L = 4.0$, all earthquake triggered landslides were remapped one week after the main event. This work proved the geographical connection between seven re-triggered slides with a volume increase of 10%, and two events of local magnitudes 4.1 and 4.0 in the Alfios area.

Four types of earthquake triggered landslides are recognized from 47 fault scarps sites.

Type A: Slides originating along step-type scarps, triggered by the main event and re-triggered by aftershocks. In this type of slide, four mobilization types are observed (Fig. 8 type A): spalling-off masses (a), peeling-off sheets (b), wedge-shaped slides (c) and tension cracks at the near-top point of the scarp (d). The original free face was steeper than 60° .

Type B: Slides, geographically isolated, originating during the third day after the main event by toppling and wedge failure on one fault (Fig. 8 type B) as a result of aftershock activity. These slides were triggered by rain showers indicating some control by climatic factors. The original free face was about 60° .

Type C: Slides (Fig. 8 type C), forming tear-drop talus triggered by the main event in structurally simple areas, denuding the free face of the fault by wedge failure.

Type D: Slides (Fig. 8 type D), originating over a shallow detachment plane and restricted to slopes modified by human activities.

The strong structural control on the slopes of the Pyrgos countryside together with the typical safety factor value (F_s) of 0.9 indicates that geomorphologically the fault scarps are characterized by a condition of limiting equilibrium and thus are controlled by a retreating process. However earthquake-triggered landslides activity during the last earthquake shows that this retreating process is interrupted by refreshing processes that keep fault scarps steep, or is intensified by shallow wedging that erodes into the fault scarp.

As the magnitude of the last earthquake is comparable to the magnitude of historical earthquakes in the area, it is suggested that the geomorphological evolution of the fault scarps is controlled by alternating long term (30 years) and short term periods (10 days) of gentle retreat and intensive refreshing and/or retreating processes.

Liquefaction sites

Liquefaction on the coast at Bouka (Fig. 3 site 48) produced slumping of the shore sediments into the sea over a length of about 30 m (west side down). Inland a NNW-trending zone of ground cracks covering an area 30 m wide and 150 m long

developed (Fig. 3, site 49). At the northern end of this zone the cracks were 30 m long and 0.1 m wide, with associated mud-sand volcanoes and water escape structures. Towards the southern end of the zone the ruptures, which were 5 m long and 2–4 cm wide, became more fragmentary. This geometry with mud-sand volcanoes in the northern part and ground cracks in the southern part of the zone suggests a southeastward propagation of the liquefaction and a general ENE-lateral spreading. This direction of propagation and the en echelon geometry is similar to the liquefied zone of the 16 October 1988 $M_L = 5.9$ Vartholomio earthquake in the NW Peloponnese, close to the Pinios river mouth (unpublished data). The damage pattern resulting from both earthquakes reveals a rapid elliptical diminution of the liquefaction effects away from the epicentre (Fig. 7a).

The ENE sense of spreading is observed in all mapped sites (Fig. 3), from cracks on the ground, in asphalt covered roads, in man-made fills and by the destruction of water pipe-lines.

The mapped sense of spreading is consistent with the damage in two cemeteries in the epicentral area where tomb-stones were broken and systematically recline to the east showing an approximate east-west distribution of seismic energy. Furthermore the earthquake triggered landslides map pattern, expressed as an isopleth map (Fig. 7d), shows that two WNW-elongate areas correspond to the denser concentration of earthquake-triggered landslides. This WNW-trending concentration of landslides indicates a general decline of damage levels away from the epicentral zone and the Alfoussa and Lanthi faults. The difference between the inferred direction of soil lateral spreading (ENE) and earthquake-triggered landslides (WNW) are possibly produced by the different methods for measurement of these observations. Soil lateral spreading is directly calculated by compass measurements and the outer limits or landslides by field mapping.

Seismotectonic interpretation

The spatial distribution of aftershocks, following the main-shock, delineates three of the major structures of the Pyrgos basin.

(1) The main-shock, as well as most aftershocks, were concentrated in the 'Alfios graben'. The style of deformation and the distribution of aftershocks in the area of the Alfios cluster can be explained by the combination of the barrier theory (Das & Aki 1977; Aki 1979) with the theory and kinematics of transfer zones (e.g. Larsen 1988; Morley *et al.* 1990). This seismogenic deformation occurred in specific locations where overstepping and overlapping faults define transfer zones (*sensu* Gawthorpe & Hurst 1993). Two transfer zones, the Pyrgos relay ramp and the Alfios antithetic interference zone, define the hypocentre of the earthquake (Fig. 9a). These zones, combined with Varvasaina relay ramp and Olympia antithetic-intrabasin zone, define the main cluster of this earthquake and the main bulk of earthquake triggered landslides deposits that have been delineated in the Alfios graben. Furthermore, the basin architecture and drainage pattern are controlled by the westward tilting of the basin floor due to the Olympia antithetic-intrabasin and the Alfios antithetic-interference transfer zones (Fig. 9a).

(2) A few aftershocks are concentrated in the 'Grape graben'. This Pliocene graben was reactivated by ruptures at

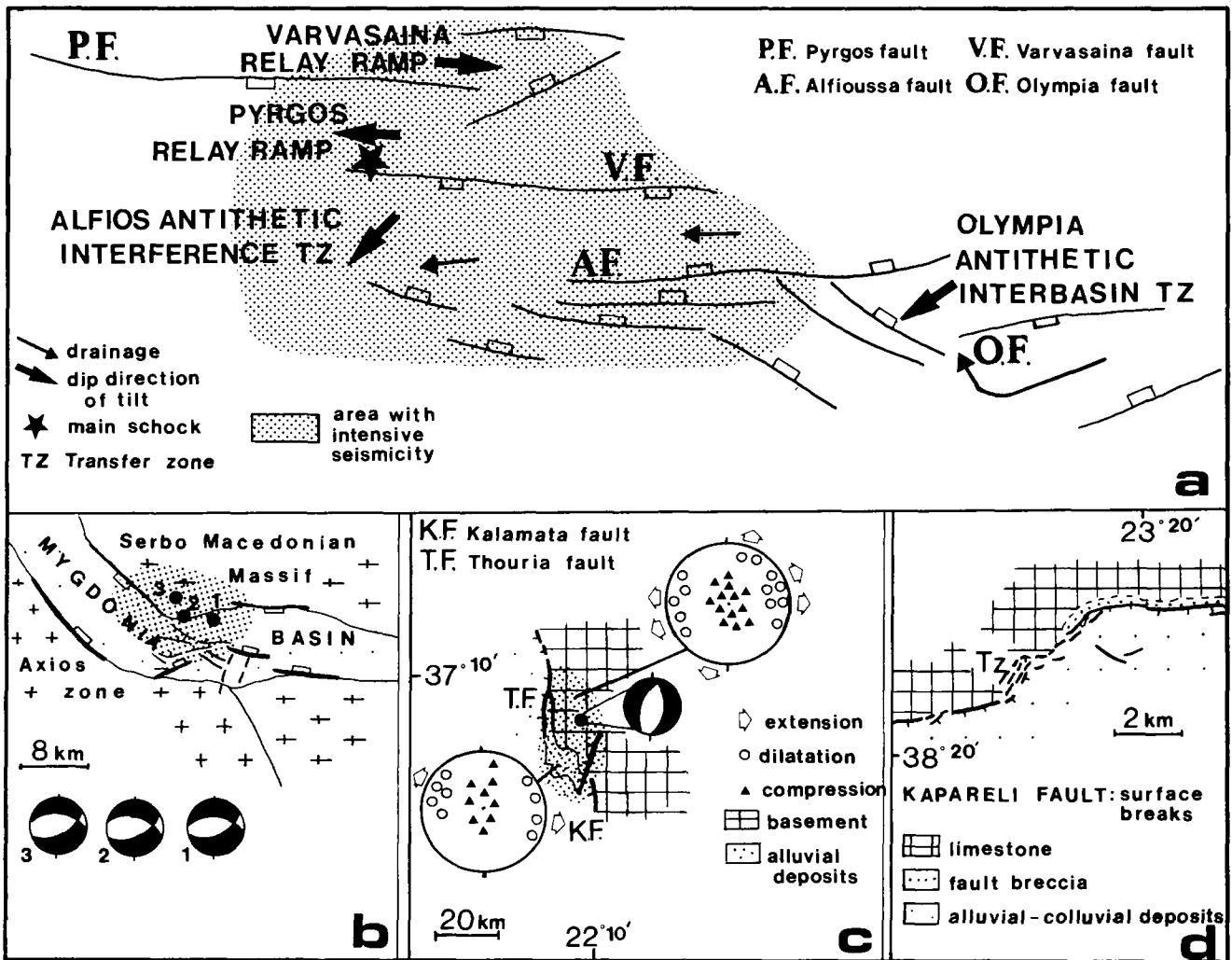


Fig. 9. Seismotectonic maps for Pyrgos (a), Thessaloniki (b), Kalamata (c) earthquakes and (d) map showing the ruptures of Kapareli fault during the Corinthian 1981 earthquake. For Thessaloniki earthquake, the transfer zone corresponds with the area of intensive seismicity. For Kalamata earthquake the transfer zone is defined at the termination between the Kalamata and Thouria faults. Focal mechanisms are shown as lower-hemisphere equal-area projections (data for Thessaloniki earthquake after Hatzfeld *et al.* 1987 and data for Kalamata earthquake after Lyon-Caen *et al.* 1988). For location of all earthquakes see Fig. 1.

depth during the last earthquake sequence with the seismogenic deformation occurring along the border faults of this graben. These faults have been active from the Pliocene to recent. Earthquake triggered landslides are scarce in the area delineated by this graben.

(3) Shallow shocks and many earthquake triggered landslide deposits define the 'Lanthi fault'.

The combination of barrier theory with the concept of transfer zones, can also be applied to understanding the tectonic setting of three other recent large earthquake sequences in Greece (Fig. 9b, c, d). Barrier theory has been used to describe the Thessaloniki earthquake (Hatzfeld *et al.* 1987), but as this area is defined between an echelon fault tip lines, it is also a transfer zone (Fig. 9b). In contrast, the proposed relay ramp of the 1986 Kalamata earthquake (Lyon-Caen *et al.* 1988) (Fig. 9c) is characterized by intense aftershock activity and so we associate this ramp with a barrier. Finally, the 1981 Corinthian earthquakes occurred in an area typically deformed by transfer zones, while

mapping of the surface ruptures indicates typical fault segmentation (Jackson *et al.* 1982) (Fig. 9d).

All these earthquakes (Fig. 9) have occurred at active zones that are characterized by both seismic and aseismic deformation, as demonstrated for central Greece by Ambraseys & Jackson (1990). Aseismic deformation (folding) around seismogenic faults is common (Roberts & Yielding 1994). Aseismic deformation at transfer zones is expected to deform the down-flexed basin floor, with the majority of deformation being concentrated close to the fault with the higher slip rate. In all the examples of Fig. 9, the aseismic deformation (folding) is expected to produce a stress concentration within the tilted basin floor, which itself will ultimately be relieved by new seismic activity, although not necessarily on the faults defining the transfer zone. The earthquake recurrence time on such newly-formed faults, which may be oblique to the original faults defining the transfer zone, will therefore depend on the slip rate of the main faults themselves.

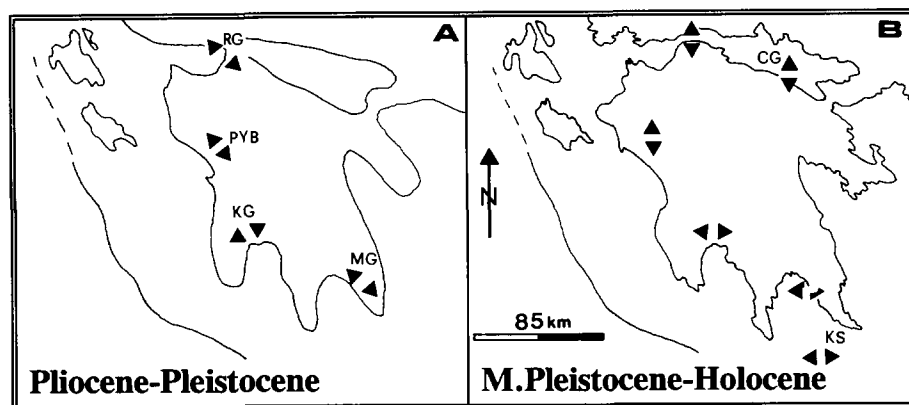


Fig. 10. Interpreted extensional palaeostress distribution in the Peloponnese. Double divergent arrowheads show direction of σ_3 determined at each site by mesoscopic analysis of fault populations (data presented in Doutsos *et al.* 1987, Doutsos *et al.* 1988, Zeligidis *et al.* 1988 and Zeligidis & Doutsos 1992). (a) For Pliocene–Pleistocene, (b) Mid-Pleistocene–Holocene. (RG) Rion graben, (PYB) Pyrgos basin, (KG) Kalama graben, (MG) Molai graben, (CG) Corinth graben, (KS) Kythira strait. Palaeocoastline in (a) after Jacobshagen (1986).

Geotectonic implications

Structural mapping and microtectonic analysis within the Pyrgos basin reveal the presence of two successive structural stages (Fig. 10).

(1) The older comprises NW- and NE-trending extensional structures formed since the Early Pliocene. The following stress distribution is proposed for this stage σ_1 : vertical, σ_2 : parallel to the NW structural trend of the Hellenides and σ_3 : normal to the structural trend of the Hellenides. In the study area, only the NE-trending set of structures remains active today, as indicated by the seismotectonic activity of the Grape graben during the Pyrgos earthquake. Further south, in the Messinia Peninsula, both fault sets are currently active, as indicated by fault displacement of marine terraces and the presence of intramountain basins filled with Pleistocene deposits (Zeligidis & Doutsos 1992). Two possible mechanisms for the formation of this fault system may be proposed: (1) Isostatic uplift as a result of crustal thickening, following the main orogenic phase which affected the West Hellenides in the mid-Miocene (Doutsos *et al.* 1988). (2) Uplift caused by underplating of sediments beneath the South Hellenic forearc in the southwest Peloponnese (see Le Pichon 1982).

(2) The younger structural stage comprises WNW- and NNE-trending normal faults typical of the recent evolution of the Aegean back arc basin. The Alfios–Pyrgos seismogenic graben, described here, is probably similar to the embryonic stage of several other seismogenic grabens in central Greece (e.g. Corinthos graben, Atalanti graben etc.). However, the prevalence of NNE-trending active faults in the southern Peloponnese, such as the Molai graben (Fig. 1) and the faults in the Kythira strait (Fig. 1) requires additional explanation. They strike parallel to the convergence direction of the African and the European plates in the area between the Peloponnese and Crete (Armijo *et al.* 1992; Jackson 1994), as has been observed in other foreland areas (Hancock & Bevan 1987) but it is not our intention to discuss them further here.

Conclusions

(1) Foreshock and aftershock sequences during the Pyrgos earthquake demonstrate the reactivation of a structurally complex area. However, most aftershocks are concentrated along the Pyrgos–Alfios zone. Two transfer zones, the Pyrgos relay and the Alfios antithetic-interference zone, host

the hypocentre of the earthquake. In three other earthquakes in Greece, there is a strong correspondence between epicentral areas and overlapping terminations of faults.

(2) The Alfiooussa fault, which caused the main shock, shows an average slip rate of 0.31 mm a^{-1} . Faults with average slip rates between 0.05 and 0.18 mm a^{-1} very probably hosted most aftershocks.

(3) Landslide deposits, triggered by the earthquake, define two thresholds of shaking intensities in the epicentral area, of local magnitudes 4.0 and 5.0.

(4) The Alfios–Pyrgos graben, hosted the Pyrgos earthquake and represents an embryonic stage of rifting in the western part of the Aegean back-arc basin. During the earthquake, older NE-trending extensional structures, formed by post-orogenic collapse after the main Alpine orogeny, were reactivated.

This work was supported by the Greek Organization for Earthquake Protection, Athens. The comments of G. Pe-Piper on an earlier version of the manuscript are gratefully acknowledged. We thank A. Tselentis for providing seismological data. The editing assistance of A. Roberts and the constructive reviews of W. G. Higgs, G. P. Roberts, and an anonymous referee greatly improved the manuscript. The constructive and helpful comments of D. J. W. Piper on all versions of this work were valuable for the final presentation. We are grateful to O. Oncken for providing the latest version of his computer program for determining stress tensors from fault striation analysis. Correspondence to I. Koukouvelas (e-mail: tdoutsos@upatras.gr).

References

- AKI, K. 1979. Characterization of barriers on an earthquake fault. *Journal of Geophysical Research*, **84**, 6140–6148.
- AMBRASEYS, N. N. & JACKSON, J. A. 1990. Seismicity and associated strain of central Greece between 1890 and 1988. *Geophysical Journal*, **101**, 663–708.
- ANDRONOPOULOS, B. & KOUKIS, G. 1977. *Engineering geology study in the area of Kremasti's monastery (Peloponnese)*. Institute of Geological and Mineral Exploration, Report 5.
- ARMIJO, R., LYON-CAEN, H. & PAPANASTASIOU, D. 1992. East–west extension and Holocene normal-fault scarps in the Hellenic arc. *Geology*, **20**, 491–494.
- CAREY, E. & BRUNIER, B. 1974. Analyse theorique et numerique d'un modele mecanique elementaire applique a l'etude d'une population de failles. *Comptes Rendus de l'Academie des Sciences Paris*, **D279**, 891–894.
- DAS, S. & AKI, K. 1977. Fault Plain With Barriers: A Versatile Earthquake Model. *Journal of Geophysical Research*, **82**, 5658–5669.

- DOUTSOS, T. & PIPER, D.J.W. 1990. Listric faulting, sedimentation and morphological evolution of the Quaternary eastern Corinth rift, Greece: First stages of continental rifting. *Geological Society of America Bulletin*, **102**, 812–829.
- & POULIMENOS, G. 1992. Geometry and kinematics of active faults and their seismotectonic significance in the western Corinth–Patras rift (Greece). *Journal of Structural Geology*, **14**, 689–699.
- , KONTOPoulos, N. & FRYDAS, D. 1987. Neotectonic evolution of northwestern continental Greece. *Geologische Rundschau*, **76**, 433–450.
- , — & POULIMENOS, G. 1988. The Corinth–Patras rift as the initial stage of continental fragmentation behind an active island arc (Greece). *Basin Research*, **1**, 177–190.
- ETCHECOPAR, A., VASSEUR, G. & DAIGNIERES, M. 1981. An inverse problem in microtectonics for the determination of the stress tensors from fault striation analysis. *Journal of Structural Geology*, **3**, 51–65.
- FRYDAS, D. 1987. Kalkiges Nannoplankton aus dem Neogen von NW-Peloponnes. *Neus Jahrbuch für Geologie und Paläontologie Monatshefte*, **5**, 274–286.
- GAWTHORPE, R. L. & HURST, J. M. 1993. Transfer zones in extensional basins: their structural style and influence on drainage development and stratigraphy. *Journal of the Geological Society, London*, **150**, 1137–1152.
- HAGEMAN, J. 1976. Stratigraphy and sedimentary history of the Upper Cenozoic of the Pyrgos-area (Western-Peloponnesus), Greece. *Annales Geologiques des pays Helleniques*, **28**, 299–333.
- HANCOCK, P. L. & BEVAN, T. G. 1987. Brittle models of foreland extension. In: COWARD, M.P., DEWEY, J. F. & HANCOCK, P. L. (eds) *Continental Extensional Tectonics*. Geological Society, London, Special Publications, **28**, 127–137.
- HATZFELD, D. 1994. On the shape of the subducting slab beneath the Peloponnese, Greece. *Geophysical Research Letters*, **21**, 173–176.
- , CHRISTODOULOU, A., SCORDILIS, E., PANAGIOTOPOULOS, D. & HATZIDIMITRIOU, P. 1987. A microearthquake study of the Mygdonian graben (N. Greece). *Earth and Planetary Science Letters*, **81**, 379–396.
- *et al.* 1989. The Hellenic subduction beneath the Peloponnese: first results of a microearthquake study. *Earth and Planetary Science Letters*, **93**, 283–291.
- , PEDOTTI, G., HATZIDIMITRIOU, P. & MAKROPOULOS, K. 1990. The strain pattern in the western Hellenic arc deduced from a microearthquake survey. *Geophysical Journal*, **101**, 181–202.
- HOEK, E. & BRAY, J. 1977. *Rock Slope Engineering*. The institution of Mining and Metallurgy, London.
- JACKSON, J. A. 1994. Active Tectonics of the Aegean Region. *Annual Review Earth and Planetary Science Letters*, **22**, 239–271.
- & MCKENZIE, D. P. 1988. Rates of active deformation in the Aegean Sea and surrounding regions. *Basin Research*, **1**, 121–128.
- , GAGNEPAIN, J., HOUSEMAN, G., KING, G. C. P., PAPADIMITRIOU, P., SOUFLERIS, C. & VIREUX, J. 1982. Seismicity and the geomorphological development of the Gulf of Corinth (Greece): the Corinth earthquakes of February and March 1981. *Earth and Planetary Science Letters*, **57**, 377–397.
- JACOBSSHAGEN, V. 1986. *Geologie von Griechenland*. Borntraeger, Berlin.
- IAEG Commission on Landslides 1990. Suggested nomenclature for landslides. *Bulletin International Association Engineering Geology*, **41**, 13–16.
- KAMBERIS, G. 1987. *Geology and Petroleum geology of NW Peloponnesus*. PhD Thesis, National Technical University, Athens.
- KEEFER, D. K. 1984. Landslides caused by earthquakes. *Geological Society of America Bulletin*, **95**, 406–421.
- KLEINHOLTER, K. 1994. *Die Neogenen Floren der Peloponnes*. PhD Thesis, Westfälischen Wilhelms Universität Münster.
- LARSEN, P. H. 1988. Relay structures in a Lower Permian basement-involved extension system, East Greenland. *Journal of Structural Geology*, **10**, 3–18.
- LEE, W. H. K. & LAHR, J. C. 1972. *HYP071: A computer program for determining hypocenter, magnitude, and first motion pattern of local earthquakes*. US Geological Survey Open File Report, 75–311.
- LE PICHON, X. 1982. Land-locked oceanic basins and continental collision: The Eastern Mediterranean as a case example. In: HSÜ, K. (ed.) *Mountain Building Processes*. Academic Press, 201–211.
- & ANGELIER, J. 1979. The Hellenic arc and trench system: a key to the neotectonic evolution of the eastern Mediterranean area. *Tectonophysics*, **60**, 1–42.
- LEYDECKER, G., BERCKHEMER, H. & DELIBASSIS, N. 1978. A study of seismicity in the Peloponnese region by precise hypocenter determinations. In: CLOSS, H., ROEDER, D. & SCHMIDT, K. (eds) *Alps, Appenines, Hellenides*. Verlagbuchhandlung, Stuttgart, 406–410.
- LYON-CAEN, H., ARMJO, R., DRAKOPOULOS, J. ET AL. 1988. The Kalamata (south Peloponnese) earthquake: detailed study of a normal fault and tectonic implication. *Journal of Geophysical Research*, **93**, 14967–15000.
- MCKENZIE, D. P. 1972. Active tectonics of the Mediterranean region. *Royal Astronomical Society Geophysical Journal*, **30**, 109–182.
- 1978. Active tectonics of the Alpine-Himalayan belt: the Aegean Sea and the surrounding regions. *Royal Astronomical Society Geophysical Journal*, **55**, 217–254.
- MERCIER, J. L., BOUSQUET, B., DELIBASSIS, N., DRAKOPOULOS, I., KERAUDREN, B., LEMELLE, F. & SOREL, D. 1972. Deformations en compression dans le quaternaire de rivages ioniens (Cephalonie, Greece). Données neotectoniques's et seismiques. *Comptes Rendus de l' Akademie des Sciences*, **275**, 2307–2310.
- MORLEY, C. K., NELSON, R. A., PATTON, T. L. & MUNN, S. G. 1990. Transfer zones in the East African Rift System and their relevance to hydrocarbon exploration in rifts. *American Association of Petroleum Geologists Bulletin*, **74**, 1234–1253.
- MOUTZOS, T. 1990. *Palynologische Untersuchungen zur Palaoklimatologie und stratigraphie der postorogen sedimente des NW-Peloponnes*. PhD Thesis, University of Munster.
- ONCKEN, O. 1988. Aspects of the reconstruction of the stress history of a fold and thrust belt (Rhenish Massif, Federal Republic of Germany). *Tectonophysics*, **152**, 19–40.
- PAPATHEODOROU, G. & FERENTINOS, G. 1993. Sedimentation processes and basin-filling depositional architecture in an active asymmetric graben: Strava graben, Gulf of Corinth, Greece. *Basin Research*, **5**, 235–253.
- PAPAZACHOS, B. C. & COMNINAKIS, P. E. 1971. Geophysical and tectonic features of the Aegean arc. *Journal of Geophysical Research*, **76**, 8517–8533.
- & — 1982. *A catalogue of earthquakes in Greece and surrounding area for the period 1901–1980*. Publications of Geophysical Laboratory University of Thessaloniki, **5**, Thessaloniki.
- & PAPAZACHOU, K. 1989. *Earthquakes in Greece*. Ziti Publications.
- RICHTER, C. F. 1935. An instrumental earthquake magnitude scale. *Bulletin of the Seismological Society of America*, **25**, 1–32.
- ROBERTS, A. M. & YIELDING, G. 1994. Continental extensional tectonics. In: HANCOCK, P. L. (eds) *Continental Deformation*. Pergamon Press, 223–250.
- ROBERTS, G. P., GAWTHORPE, R. L. & STEWART, I. S. 1993. Surface faulting within active normal fault zones: examples from the Gulf of Corinth fault system, Central Greece. *Zeitschrift für Geomorphologie NF*, **94**, 303–328.
- ROBERTS, S. & JACKSON, J. A. 1991. Active normal faulting in central Greece: an overview. In: ROBERTS, A. M., YIELDING, G. & FREEMAN, B. (eds) *The Geometry of Normal Faults*. Geological Society, London, Special Publications, **56**, 125–142.
- SCHOLZ, C. H. 1990. *The mechanics of earthquakes and faulting*. Cambridge University Press.
- SKEMPTON, A. W. & DELORY, F. A. 1957. Stability of natural slopes in London clay. *Proceedings of 4th International Conference on Soil Mechanics Foundation Engineering, London*, **2**, 378–381.
- STRAHLER, A. N. 1975. *Physical Geography* (4th edition). John Wiley, New York.
- SYMEONIDIS, N., THEODOROU, G., SCHUTT, H. & VELITZELIS, E. 1987. Paleontological and stratigraphic observations in the area of Achaia and Etoloakarnania (W. Greece). *Annales Geologiques des Pays Helleniques*, **38**, 317–353.
- TERZAGHI, K. 1950. *Mechanism of landslides. Application of engineering to geology* (Berkey Volume). *Geological Society of America*, 83–123.
- TSAILA-MONOPOLIS, S., IOAKEIM, X. & KAMPERIS, E. 1993. Biostratigraphical correlation in the Neogene and Quaternary sediments in the Katakolon oil wells, (NW Peloponnese). *Memorial volume for Professor Panagos*, National Technical University Athens, 813–828.
- UNDERHILL, J. R. 1989. Late Cenozoic deformation of the Hellenide foreland, western Greece. *Geological Society of America Bulletin*, **101**, 613–634.
- ZELLIDIS, A. & DOUTSOS, T. 1992. An interference pattern of Neotectonic faults in the southwestern part of the Hellenic Forearc basin, Greece. *Zeitschrift der Deutschen Geologischen Gesellschaft*, **143**, 95–105.
- , KOUKOUVELAS, I. K. & DOUTSOS, T. 1988. Neogene paleostress changes behind the forearc fold belt in the Patraikos Gulf area, western Greece. *Neues Jahrbuch für Geologie und Paläontologie Monatshefte*, **5**, 311–325.